



Universiteit
Leiden
The Netherlands

Hitomi (ASTRO-H) X-ray Astronomy Satellite

Kaastra, J.S.; et al.

Citation

Kaastra, J. S. (2018). Hitomi (ASTRO-H) X-ray Astronomy Satellite. *Journal Of Astronomical Telescopes, Instruments, And Systems*, 4(2), 021402. doi:10.1117/1.JATIS.4.2.021402

Version: Not Applicable (or Unknown)

License: [Leiden University Non-exclusive license](#)

Downloaded from: <https://hdl.handle.net/1887/70899>

Note: To cite this publication please use the final published version (if applicable).

Journal of Astronomical Telescopes, Instruments, and Systems

AstronomicalTelescopes.SPIEDigitalLibrary.org

Hitomi (ASTRO-H) X-ray Astronomy Satellite

Tadayuki Takahashi
Motohide Kokubun
Kazuhiisa Mitsuda
Richard L. Kelley
Takaya Ohashi
Felix Aharonian
Hiroki Akamatsu
Fumie Akimoto
Steven W. Allen
Naohisa Anabuki
Lorella Angelini
Keith Arnaud
Makoto Asai
Marc Audard
Hisamitsu Awaki
Magnus Axelsson
Philipp Azzarello
Chris Baluta
Aya Bamba
Nobutaka Bando
Marshall W. Bautz
Thomas Bialas
Roger Blandford
Kevin Boyce
Laura W. Brenneman
Gregory V. Brown
Esra Bulbul
Edward M. Cackett
Edgar Canavan
Maria Chernyakova
Meng P. Chiao
Paolo S. Coppi
Elisa Costantini
Steve O' Dell
Michael DiPirro
Chris Done
Tadayasu Dotani
John Doty
Ken Ebisawa
Megan E. Eckart
Teruaki Enoto
Yuichiro Ezoe
Andrew C. Fabian
Carlo Ferrigno
Adam R. Foster
Ryuichi Fujimoto
Yasushi Fukazawa
Stefan Funk
Akihiro Furuzawa
Massimiliano Galeazzi
Luigi C. Gallo
Poshak Gandhi
Kirk Gilmore
Margherita Giustini
Andrea Goldwurm
Liyi Gu
Matteo Guainazzi
Daniel Haas
Yoshito Haba
Kouichi Hagino
Kenji Hamaguchi
Ilana M. Harrus
Isamu Hatsukade
Takayuki Hayashi
Katsuhiro Hayashi
Kiyoshi Hayashida
Jan-Willem den Herder
Junko S. Hiraga
Kazuyuki Hirose
Ann Hornschemeier
Akio Hoshino
John P. Hughes
Yuto Ichinohe
Ryo Iizuka
Hajime Inoue
Yoshiyuki Inoue
Kazunori Ishibashi
Manabu Ishida
Kumi Ishikawa
Kosei Ishimura
Yoshitaka Ishisaki
Masayuki Itoh
Masachika Iwai
Naoko Iwata
Naoko Iyomoto
Chris Jewell
Jelle Kaastra
Tim Kallman
Tsuneyoshi Kamae
Erin Kara
Jun Kataoka
Satoru Katsuda
Junichiro Katsuta
Madoka Kawaharada
Nobuyuki Kawai
Taro Kawano
Shigeo Kawasaki
Dmitry Khangulyan
Caroline A. Kilbourne
Mark Kimball
Ashley King
Takao Kitaguchi
Shunji Kitamoto
Tetsu Kitayama
Takayoshi Kohmura
Saori Konami
Tatsuro Kosaka
Alex Koujelev
Katsuji Koyama
Shu Koyama
Peter Kretschmar
Hans A. Krimm
Aya Kubota
Hideyo Kunieda
Philippe Laurent
Shiu-Hang Lee
Maurice A. Leutenegger
Olivier Limousin
Michael Loewenstein
Knox S. Long
David Lumb
Greg Madejski
Yoshitomo Maeda
Daniel Maier
Kazuo Makishima
Maxim Markevitch
Candace Masters
Hironori Matsumoto
Kyoko Matsushita
Dan McCammon
Daniel Mcguinness
Brian R. McNamara
Missagh Mehdipour
Joseph Miko
Eric D. Miller
Jon M. Miller
Shin Mineshige
Kenji Minesugi
Ikuyuki Mitsuiishi
Takuya Miyazawa
Tsunefumi Mizuno
Hideyuki Mori
Koji Mori
Franco Moroso
Harvey Moseley
Theodore Muench
Koji Mukai
Hiroshi Murakami
Toshio Murakami
Richard F. Mushotzky
Housei Nagano
Ryo Nagino
Takao Nakagawa
Hiroshi Nakajima
Takeshi Nakamori
Toshio Nakano
Shinya Nakashima
Kazuhiro Nakazawa
Yoshiharu Namba
Chikara Natsukari
Yusuke Nishioka
Kumiko K. Nobukawa
Masayoshi Nobukawa
Hirofumi Noda
Masaharu Nomachi
Hirokazu Odaka
Hiroyuki Ogawa
Mina Ogawa
Keiji Ogi
Masanori Ohno
Masayuki Ohta
Takashi Okajima
Atsushi Okamoto
Tsuyoshi Okazaki
Naomi Ota
Masanobu Ozaki
Frits Paerels
Stéphane Paltani
Arvind Parmar
Robert Petre
Ciro Pinto
Jelle de Plaa
Martin Pohl
James Pontius
Frederick S. Porter
Katja Pottschmidt
Brian Ramsey
Christopher Reynolds
Helen Russell
Samar Safi-Harb
Shinya Saito
Kazuhiro Sakai
Shin-ichiro Sakai
Hiroaki Sameshima
Toru Sasaki
Goro Sato
Kosuke Sato
Rie Sato
Yoichi Sato
Makoto Sawada
Norbert Schartel
Peter J. Serlemitsos
Hiromi Seta
Yasuko Shibano
Maki Shida
Megumi Shidatsu
Takanobu Shimada
Keisuke Shinozaki
Peter Shirron
Aurora Simionescu
Cynthia Simmons
Randall K. Smith
Gary Sneiderman
Yang Soong
Lukasz Stawarz
Yasuharu Sugawara
Satoshi Sugita
Hiroyuki Sugita
Andrew Szymkowiak
Hiroyasu Tajima
Hiromitsu Takahashi
Shin'ichiro Takeda
Yoh Takei
Toru Tamagawa
Takayuki Tamura
Keisuke Tamura
Takaaki Tanaka
Yasuo Tanaka
Yasuyuki T. Tanaka
Makoto S. Tashiro
Yuzuru Tawara
Yukikatsu Terada
Yuichi Terashima
Francesco Tombesi
Hiroshi Tomida
Yohko Tsuboi
Masahiro Tsujimoto
Hiroshi Tsunemi
Takeshi Go Tsuru
Hiroyuki Uchida
Hideki Uchiyama
Yasunobu Uchiyama
Shutaro Ueda
Yoshihiro Ueda
Shiro Ueno
Shin'ichiro Uno
C. Megan Urry
Eugenio Ursino
Cor P. de Vries
Atsushi Wada
Shin Watanabe
Tomomi Watanabe
Norbert Werner
Daniel R. Wik
Dan R. Wilkins
Brian J. Williams
Shinya Yamada
Takahiro Yamada
Hiroya Yamaguchi
Kazutaka Yamaoka
Noriko Y. Yamasaki
Makoto Yamauchi
Shigeo Yamauchi
Tahir Yaqoob
Yoichi Yatsu
Daisuke Yonetoku
Atsumasa Yoshida
Takayuki Yuasa
Irina Zhuravleva
Abderahmen Zoghbi

SPiE

Tadayuki Takahashi et al., "Hitomi (ASTRO-H) X-ray Astronomy Satellite," *J. Astron. Telesc. Instrum. Syst.* 4(2), 021402 (2018), doi: 10.1117/1.JATIS.4.2.021402.

Hitomi (ASTRO-H) X-ray Astronomy Satellite

Tadayuki Takahashi,^{a,*} Motohide Kokubun,^a Kazuhisa Mitsuda,^a Richard L. Kelley,^b Takaya Ohashi,^c Felix Aharonian,^{d,e,f} Hiroki Akamatsu,^g Fumie Akimoto,^h Steven W. Allen,^{i,j,k} Naohisa Anabuki,^l Lorella Angelini,^b Keith Arnaud,^m Makoto Asai,^k Marc Audard,ⁿ Hisamitsu Awaki,^o Magnus Axelsson,^p Philipp Azzarello,ⁿ Chris Baluta,^a Aya Bamba,^{q,r} Nobutaka Bando,^a Marshall W. Bautz,^s Thomas Bialas,^b Roger Blandford,^{i,j,k} Kevin Boyce,^b Laura W. Brenneman,^t Gregory V. Brown,^u Esra Bulbul,^s Edward M. Cackett,^v Edgar Canavan,^b Maria Chernyakova,^d Meng P. Chiao,^b Paolo S. Coppi,^{w,x} Elisa Costantini,^g Steve O' Dell,^b Michael DiPirro,^b Chris Done,^y Tadayasu Dotani,^a John Doty,^z Ken Ebisawa,^a Megan E. Eckart,^b Teruaki Enoto,^{aa,ab} Yuichiro Ezoe,^c Andrew C. Fabian,^{ac} Carlo Ferrigno,ⁿ Adam R. Foster,^t Ryuichi Fujimoto,^{ad} Yasushi Fukazawa,^{ae} Stefan Funk,^{af} Akihiro Furuzawa,^{ag} Massimiliano Galeazzi,^{ah} Luigi C. Gallo,^{ai} Poshak Gandhi,^{aj} Kirk Gilmore,ⁱ Margherita Giustini,^g Andrea Goldwurm,^{ak,al} Liyi Gu,^{am} Matteo Guainazzi,^{an} Daniel Haas,^g Yoshito Haba,^{ao} Kouichi Hagino,^{ap} Kenji Hamaguchi,^{b,m} Ilana M. Harrus,^{b,m} Isamu Hatsukade,^{aq} Takayuki Hayashi,^{ar} Katsuhiro Hayashi,^{a,ar} Kiyoshi Hayashida,^l Jan-Willem den Herder,^g Junko S. Hiraga,^{as} Kazuyuki Hirose,^a Ann Hornschemeier,^b Akio Hoshino,^{at} John P. Hughes,^{au} Yuto Ichinohe,^c Ryo Iizuka,^a Hajime Inoue,^{av} Yoshiyuki Inoue,^{am} Kazunori Ishibashi,^{ar} Manabu Ishida,^a Kumi Ishikawa,^a Kosei Ishimura,^a Yoshitaka Ishisaki,^c Masayuki Itoh,^{aw} Masachika Iwai,^a Naoko Iwata,^a Naoko Iyomoto,^{ax} Chris Jewell,^{ay} Jelle Kaastra,^{g,az} Tim Kallman,^b Tsuneyoshi Kamae,^q Erin Kara,^m Jun Kataoka,^{ba} Satoru Katsuda,^{bb,bc} Junichiro Katsuta,^{ae} Madoka Kawaharada,^{bd} Nobuyuki Kawai,^{be} Taro Kawano,^a Shigeo Kawasaki,^a Dmitry Khangulyan,^{at} Caroline A. Kilbourne,^b Mark Kimball,^b Ashley King,^l Takao Kitaguchi,^{ae} Shunji Kitamoto,^{at} Tetsu Kitayama,^{bf} Takayoshi Kohmura,^{ap} Saori Konami,^c Tatsuro Kosaka,^{bg} Alex Koujelev,^{bh} Katsuji Koyama,^{bi} Shu Koyama,^a Peter Kretschmar,^{bj} Hans A. Krimm,^{bk,bl} Aya Kubota,^{bm} Hideyo Kunieda,^{ar} Philippe Laurent,^{ak,al} Shiu-Hang Lee,^{aa} Maurice A. Leutenegger,^b Olivier Limousin,^{al} Michael Loewenstein,^{b,bn} Knox S. Long,^{bo} David Lumb,^{an} Greg Madejski,ⁱ Yoshitomo Maeda,^a Daniel Maier,^{ak,al} Kazuo Makishima,^{bp} Maxim Markevitch,^b Candace Masters,^b Hironori Matsumoto,^l Kyoko Matsushita,^{bq} Dan McCammon,^{br} Daniel Mcguinness,^b Brian R. McNamara,^{bs} Missagh Mehdipour,^g Joseph Miko,^b Eric D. Miller,^s Jon M. Miller,^{bt} Shin Mineshige,^{aa} Kenji Minesugi,^a Ikuyuki Mitsuishi,^{ar} Takuya Miyazawa,^{bu} Tsunefumi Mizuno,^{ae,bv} Hideyuki Mori,^b Koji Mori,^{aq} Franco Moroso,^{bh} Harvey Moseley,^b Theodore Muench,^b Koji Mukai,^{b,m} Hiroshi Murakami,^{bw} Toshio Murakami,^{ad} Richard F. Mushotzky,^{bn} Husei Nagano,^{bx} Ryo Nagino,^l Takao Nakagawa,^a Hiroshi Nakajima,^l Takeshi Nakamori,^{by} Toshio Nakano,^{am} Shinya Nakashima,^{bp} Kazuhiro Nakazawa,^{q,r} Yoshiharu Namba,^{bz} Chikara Natsukari,^a Yusuke Nishioka,^{aq} Kumiko K. Nobukawa,^{ca} Masayoshi Nobukawa,^{cb} Hirofumi Noda,^{cc,cd} Masaharu Nomachi,^{ce} Hirokazu Odaka,^l Hiroyuki Ogawa,^a Mina Ogawa,^a Keiji Ogi,^o Masanori Ohno,^{ae} Masayuki Ohta,^a Takashi Okajima,^b Atsushi Okamoto,^{bd} Tsuyoshi Okazaki,^a Naomi Ota,^{ca} Masanobu Ozaki,^a Frits Paerels,^{cf} Stéphane Paltani,ⁿ Arvind Parmar,^{av} Robert Petre,^b Ciro Pinto,^{ac} Jelle de Plaa,^g Martin Pohl,ⁿ James Pontius,^b Frederick S. Porter,^b Katja Pottschmidt,^{b,m} Brian Ramsey,^b Christopher Reynolds,^{bn} Helen Russell,^{ac} Samar Safi-Harb,^{cg} Shinya Saito,^{at} Kazuhiro Sakai,^b Shin-ichiro Sakai,^a Hiroaki Sameshima,^a Toru Sasaki,^{bq} Goro Sato,^a Kosuke Sato,^{bq,bc} Rie Sato,^a Yoichi Sato,^{bd} Makoto Sawada,^{ch} Norbert Schartel,^{bj} Peter J. Serlemitsos,^b Hiromi Seta,^c Yasuko Shibano,^a Maki Shida,^a Megumi Shidatsu,^{bp} Takanobu Shimada,^a Keisuke Shinozaki,^{bd} Peter Shirron,^b Aurora Simionescu,^a Cynthia Simmons,^b Randall K. Smith,^t Gary Sneiderman,^b Yang Soong,^b Łukasz Stawarz,^{ci} Yasuharu Sugawara,^a Satoshi Sugita,^{be} Hiroyuki Sugita,^{bd} Andrew Szymkowiak,^x Hiroyasu Tajima,^h Hiromitsu Takahashi,^{ae} Shin'ichiro Takeda,^{bu} Yoh Takei,^a Toru Tamagawa,^{am} Takayuki Tamura,^a Keisuke Tamura,^{ar} Takaaki Tanaka,^{bi} Yasuo Tanaka,^{cj,a} Yasuyuki T. Tanaka,^{ae} Makoto S. Tashiro,^{a,bc} Yuzuru Tawara,^{ar} Yukikatsu Terada,^{bc} Yuichi Terashima,^o Francesco Tombesi,^{b,m,ck} Hiroshi Tomida,^a Yohko Tsuboi,^{bb} Masahiro Tsujimoto,^a Hiroshi Tsunemi,^l Takeshi Go Tsuru,^{bi} Hiroyuki Uchida,^{bi} Hideki Uchiyama,^{ci} Yasunobu Uchiyama,^{at} Shutaro Ueda,^a Yoshihiro Ueda,^{aa} Shiro Ueno,^a Shin'ichiro Uno,^{cm} C. Megan Urry,^x Eugenio Ursino,^{ah} Cor P. de Vries,^g Atsushi Wada,^a Shin Watanabe,^a Tomomi Watanabe,^b Norbert Werner,^{ae,cn,co} Daniel R. Wik,^{b,cp,cq} Dan R. Wilkins,ⁱ Brian J. Williams,^{bo} Shinya Yamada,^c Takahiro Yamada,^a Hiroya Yamaguchi,^{b,bn} Kazutaka Yamaoka,^{h,ar} Noriko Y. Yamasaki,^a Makoto Yamauchi,^{aq} Shigeo Yamauchi,^{ca} Tahir Yaqoob,^{b,m} Yoichi Yatsu,^{be} Daisuke Yonetoku,^{ad} Atsumasa Yoshida,^{ch} Takayuki Yuasa,^{am} Irina Zhuravleva,^{ij} and Abderahmen Zoghbi^{bt}

^aJapan Aerospace Exploration Agency, Institute of Space and Astronautical Science, Sagamihara, Kanagawa, Japan

^bNASA, Goddard Space Flight Center, Greenbelt, Maryland, United States

^cTokyo Metropolitan University, Department of Physics, Hachioji, Tokyo, Japan

^dDublin Institute for Advanced Studies, Dublin 2, Ireland

^eMax-Planck-Institut für Kernphysik, Heidelberg, Germany

^fGran Sasso Science Institute, L'Aquila (AQ), Italy

^gSRON Netherlands Institute for Space Research, Utrecht, The Netherlands

^hNagoya University, Institute for Space-Earth Environmental Research, Nagoya, Aichi, Japan

ⁱStanford University, Kavli Institute for Particle Astrophysics and Cosmology, Stanford, California, United States

^jStanford University, Department of Physics, Stanford, California, United States

^kSLAC National Accelerator Laboratory, Menlo Park, California, United States

^lOsaka University, Department of Earth and Space Science, Toyonaka, Osaka, Japan

^mUniversity of Maryland, Department of Physics, Baltimore, Maryland, United States

ⁿUniversity of Geneva, Department of Astronomy, Versoix, Switzerland

^oEhime University, Department of Physics, Matsuyama, Ehime, Japan

^pStockholm University, Oskar Klein Center, Department of Physics, Stockholm, Sweden

^qThe University of Tokyo, Department of Physics, Tokyo, Japan

- ^TThe University of Tokyo, Research Center for the Early Universe, School of Science, Tokyo, Japan
^SMassachusetts Institute of Technology, Kavli Institute for Astrophysics and Space Research, Cambridge, Massachusetts, United States
^ISmithsonian Astrophysical Observatory, Cambridge, Massachusetts, United States
^LLawrence Livermore National Laboratory, Livermore, California, United States
^WWayne State University, Department of Physics and Astronomy, Detroit, Michigan, United States
^YYale University, Department of Astronomy, New Haven, Connecticut, United States
^XYale University, Department of Physics, New Haven, Connecticut, United States
^UUniversity of Durham, Centre for Extragalactic Astronomy, Department of Physics, Durham, United Kingdom
^NNoqsj Aerospace Ltd., Pine, Colorado, United States
^aKyoto University, Department of Astronomy, Sakyo-ku, Kyoto, Japan
^{ab}Kyoto University, The Hakubi Center for Advanced Research, Kyoto, Japan
^{ac}University of Cambridge, Institute of Astronomy, Cambridge, United Kingdom
^{ad}Kanazawa University, Faculty of Mathematics and Physics, Kanazawa, Ishikawa, Japan
^{ae}Hiroshima University, School of Science, Higashi-Hiroshima, Japan
^{af}Friedrich-Alexander-Universität Erlangen-Nürnberg, Erlangen Centre for Astroparticle Physics, Erlangen, Germany
^{ag}Fujita Health University, Toyoake, Aichi, Japan
^{ah}University of Miami, Physics Department, Coral Gables, Florida, United States
^{ai}Saint Mary's University, Department of Astronomy and Physics, Halifax, Nova Scotia, Canada
^{aj}University of Southampton, Department of Physics and Astronomy, Highfield, Southampton, United Kingdom
^{ak}Laboratoire APC, Paris, France
^{al}CEA Saclay, Paris, France
^{am}RIKEN Nishina Center, Wako, Saitama, Japan
^{an}European Space Research and Technology Center, Noordwijk, The Netherlands
^{ao}Aichi University of Education, Department of Physics and Astronomy, Aichi, Japan
^{ap}Tokyo University of Science, Department of Physics, Noda, Chiba, Japan
^{aq}University of Miyazaki, Department of Applied Physics and Electronic Engineering, Miyazaki, Japan
^{ar}Nagoya University, Department of Physics, Nagoya, Aichi, Japan
^{as}Kwansei Gakuin University, Department of Physics, Sanda, Hyogo, Japan
^{at}Rikkyo University, Department of Physics, Toshima-ku, Tokyo, Japan
^{au}Rutgers University, Department of Physics and Astronomy, Piscataway, New Jersey, United States
^{av}Meisei University, Hino, Tokyo, Japan
^{aw}Kobe University, Graduate School of Human Development and Environment, Hyogo, Japan
^{ax}Kyushu University, Fukuoka, Japan
^{ay}European Space Agency, European Space Research and Technology Centre, Noordwijk, The Netherlands
^{az}Leiden University, Leiden Observatory, Leiden, The Netherlands
^{ba}Waseda University, Research Institute for Science and Engineering, Shinjuku, Tokyo, Japan
^{bb}Chuo University, Department of Physics, Bunkyo, Tokyo, Japan
^{bc}Saitama University, Department of Physics, Sakura-ku, Saitama, Japan
^{bd}Japan Aerospace Exploration Agency, Tsukuba Space Center, Ibaraki, Japan
^{be}Tokyo Institute of Technology, Department of Physics, Meguro-ku, Tokyo, Japan
^{bf}Toho University, Department of Physics, Funabashi, Chiba, Japan
^{bg}Kochi University of Technology, School of Systems Engineering, Kochi, Japan
^{bh}Canadian Space Agency, St-Hubert, Québec, Canada
^{bi}Kyoto University, Department of Physics, Kitashirakawa-Oiwake-Cho, Sakyo, Kyoto, Japan
^{bj}European Space Astronomy Center, Madrid, Spain
^{bk}Universities Space Research Association, Columbia, Maryland, United States
^{bl}National Science Foundation, Arlington, Virginia, United States
^{bm}Shibaura Institute of Technology, Department of Electronic Information Systems, Saitama-shi, Saitama, Japan
^{bn}University of Maryland, Department of Astronomy, College Park, Maryland, United States
^{bo}Space Telescope Science Institute, Baltimore, Maryland, United States
^{bp}Institute of Physical and Chemical Research, Wako, Saitama, Japan
^{bq}Tokyo University of Science, Department of Physics, Shinjuku-ku, Tokyo, Japan
^{br}University of Wisconsin, Department of Physics, Madison, Wisconsin, United States
^{bs}University of Waterloo, Department of Physics and Astronomy, Waterloo, Ontario, Canada
^{bt}University of Michigan, Department of Astronomy, Ann Arbor, Michigan, United States
^{bu}Okinawa Institute of Science and Technology Graduate University, Onna-son Okinawa, Japan
^{bv}Hiroshima University, Hiroshima Astrophysical Science Center, Higashi-Hiroshima, Hiroshima, Japan
^{bw}Tohoku Gakuin University, Faculty of Liberal Arts, Izumi-ku, Sendai, Miyagi, Japan
^{bx}Nagoya University, Department of Mechanical and Aerospace Engineering, Nagoya, Aichi, Japan
^{by}Yamagata University, Faculty of Science, Yamagata, Japan
^{bz}Chubu University, Department of Mechanical Engineering, Kasugai, Aichi, Japan
^{ca}Nara Women's University, Department of Physics, Nara, Japan
^{cb}Nara University of Education, Department of Teacher Training and School Education, Nara, Japan
^{cc}Tohoku University, Frontier Research Institute for Interdisciplinary Sciences, Sendai, Miyagi, Japan
^{cd}Tohoku University, Astronomical Institute, Sendai, Miyagi, Japan
^{ce}Osaka University, Research Center for Nuclear Physics, Osaka, Japan
^{cf}Columbia University, Astrophysics Laboratory, New York, New York, United States
^{cg}University of Manitoba, Department of Physics and Astronomy, Winnipeg, Manitoba, Canada
^{ch}Aoyama Gakuin University, Sagamihara, Kanagawa, Japan
^{ci}Astronomical Observatory of Jagiellonian University, Kraków, Poland
^{cj}Max-Planck-Institut für extraterrestrische Physik, Garching, Germany
^{ck}University of Rome "Tor Vergata", Department of Physics, Rome, Italy
^{cl}Shizuoka University, Faculty of Education, Shizuoka, Japan
^{cm}Nihon Fukushi University, Faculty of Health Sciences, Handa, Aichi, Japan
^{cn}MTA-Eötvös University Lendület Hot Universe Research Group, Budapest, Hungary
^{co}Masaryk University, Department of Theoretical Physics and Astrophysics, Faculty of Science, Brno, Czech Republic

^{op}University of Utah, Department of Physics and Astronomy, Salt Lake City, Utah, United States

^{oa}The Johns Hopkins University, Homewood Campus, Baltimore, Maryland, United States

Abstract. The Hitomi (ASTRO-H) mission is the sixth Japanese x-ray astronomy satellite developed by a large international collaboration, including Japan, USA, Canada, and Europe. The mission aimed to provide the highest energy resolution ever achieved at $E > 2$ keV, using a microcalorimeter instrument, and to cover a wide energy range spanning four decades in energy from soft x-rays to gamma rays. After a successful launch on February 17, 2016, the spacecraft lost its function on March 26, 2016, but the commissioning phase for about a month provided valuable information on the onboard instruments and the spacecraft system, including astrophysical results obtained from first light observations. The paper describes the Hitomi (ASTRO-H) mission, its capabilities, the initial operation, and the instruments/spacecraft performances confirmed during the commissioning operations for about a month. © The Authors. Published by SPIE under a Creative Commons Attribution 3.0 Unported License. Distribution or reproduction of this work in whole or in part requires full attribution of the original publication, including its DOI. [DOI: [10.1117/1.JATIS.4.2.021402](https://doi.org/10.1117/1.JATIS.4.2.021402)]

Keywords: x-ray; hard x-ray; gamma ray; x-ray astronomy; gamma-ray astronomy; microcalorimeter.

Paper 17063SSP received Aug. 11, 2017; accepted for publication Feb. 5, 2018; published online Mar. 13, 2018.

1 Introduction

The Hitomi (ASTRO-H) satellite was launched from Tanegashima Space Center of Japan Aerospace Exploration Agency (JAXA) at 17:45 JST on February 17, 2016 (Fig. 1). After successfully executing start-up operations, the satellite lost contact with the ground on March 26, with signatures of partial breakup of the spacecraft. On April 28, JAXA decided to discontinue the recovery operation of Hitomi. Even though the lifetime was short, the commissioning phase for about a month provided valuable information on the onboard instruments and the spacecraft system, including astrophysical results obtained from first light observations. This paper reports the mission purpose of Hitomi and the technologies achieved through the operations carried out in the commissioning phase.

Our image of the Universe has been dramatically changing from static to dynamic on many scales. X-ray measurements have efficiently detected dynamical and energetic properties of cosmic objects, based on significant improvements in the sensitivity for timing, imaging, and spectroscopic studies. High-resolution x-ray images provided by Chandra, in particular, show dynamical features in the form of shocks, cosmic jets, and outflows of hot gasses. Clusters of galaxies are the largest gravitationally bound objects in the Universe. Many of these systems are now recognized to be undergoing violent mergers characterized by shocks and cold fronts in x-ray and radio images. Supermassive black holes are found in many galaxies, surrounded by a dense gas in some cases, and their coevolution with the host galaxies over the cosmological timescale is an important issue still to be understood. Precise velocity and ionization state of the plasma within these objects, as well as heated component or emission from accelerated particles cannot be identified only by image. Breakthroughs in x-ray observation techniques would bring new views about the evolution of these objects.

High-resolution spectroscopy combined with a wideband energy coverage is a very powerful way of looking into the dynamical evolution of the Universe through x-ray observations. Energy resolution as high as $\Delta E < 7$ eV in full-width at half

maximum (FWHM) would enable to measure Doppler motions with an accuracy of ~ 100 km s⁻¹ at 6 keV and also can diagnose the detail of ionization state of metals. Sensitivity up to 600 keV, combined with imaging capability up to 80 keV, will show the highest energy regions in the spectrum and the spatial distribution of the accelerated particles. Our current knowledge on how much and in what form the nonthermal energy is produced and carried is still quite poor. The great improvements in the energy resolution and wideband coverage of Hitomi represent a substantial advance in our ability to probe all forms of energy in cosmic objects, such as clusters of galaxies and supermassive black holes. Such an improvement in x-ray astronomy also matches well with the recent progress occurring in radio and gamma-ray bands.

The Hitomi (ASTRO-H) mission has been designed to achieve these aims.^{1–8} This is an international x-ray satellite, which was launched with the 30th H-IIA rocket. NASA selected U.S. participation on ASTRO-H as a Mission of Opportunity in the Explorer Program category. Under this program, the NASA/Goddard Space Flight Center collaborates with ISAS/JAXA on the implementation of the x-ray microcalorimeter and the Soft X-ray Telescopes (SXTs) (SXS Proposal NASA/GSFC, 2007).⁹ Other institutional members of the collaboration are SRON (Netherlands Institute for Space Research), Geneva University, CEA/IRFU [French Alternative Energies and Atomic Energy Commission (CEA)/Institute of Research into the Fundamental Laws of the Universe (IRFU)], CSA (Canadian Space Agency), Stanford University, and European Space Agency. In early 2009, NASA, ESA, and JAXA selected 13 science advisors to provide scientific guidance to the ASTRO-H project. The ESA contribution to the ASTRO-H mission includes the procurement of payload hardware elements that enhance the scientific capability of the mission.

2 Spacecraft

There are four focusing telescopes mounted on the top of a fixed optical bench (FOB). Two of the four telescopes are SXTs and they have a 5.6-m focal length. They focus soft-energy x-rays ($E = 0.3$ to 12 keV) onto focal plane detectors mounted on the base plate of the spacecraft (see Fig. 2). One SXT points to a microcalorimeter spectrometer array in the Soft X-ray Spectrometer (SXS) with excellent energy resolution of < 7 eV, and the other SXT points to a large-area CCD array in the Soft

*Address all correspondence to: Tadayuki Takahashi, E-mail: takahasi@astro.isas.jaxa.jp

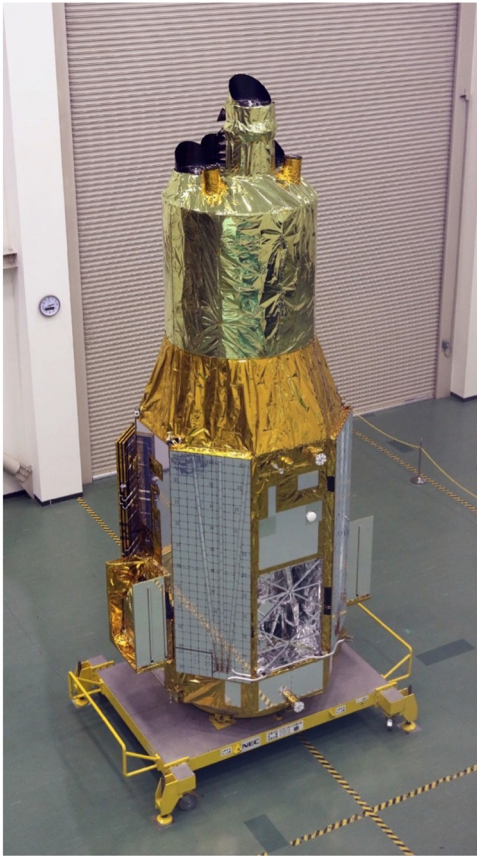


Fig. 1 A photograph of the Hitomi satellite. The height in this launch configuration is 7.86 m.

X-ray Imager (SXI). The other two telescopes are Hard X-ray Telescopes (HXTs) capable of focusing high-energy x-rays ($E = 5$ to 80 keV). The focal length of the HXTs is 12 m. The Hard X-ray Imager (HXI) consists of two detector units, which are mounted on the HXI plate, at the end of a 6-m

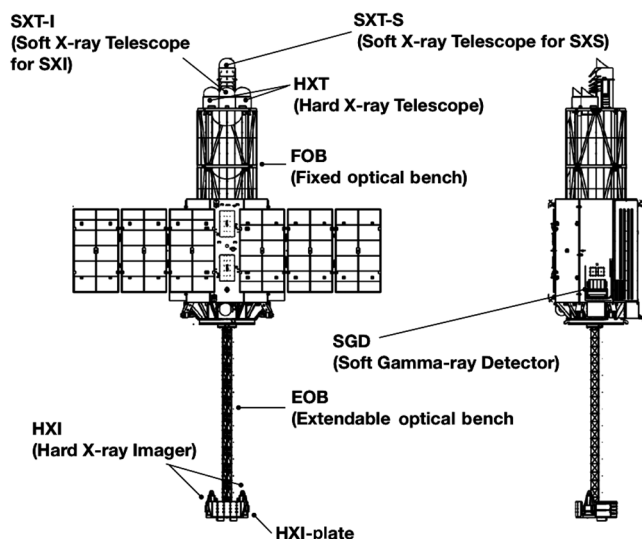


Fig. 2 Schematic view of the Hitomi satellite with the extendible optical bench deployed. The total length of the satellite is about 14 m.^{8,10-12} The SXS instrument is equipped in the opposite side of the solar paddle.

extendible optical bench (EOB) that is stowed to fit in the launch fairing and deployed once in orbit. To extend the energy coverage to the soft γ -ray region up to 600 keV, the Soft Gamma-ray Detector (SGD) was implemented as a nonfocusing detector. Two SGD detectors are mounted separately on two sides of the satellite. With these instruments, Hitomi covered the entire bandpass between 0.3 and 600 keV. The key parameters of those instruments are summarized in Table 1.

The lightweight design of the EOB renders it potentially vulnerable to distortions from thermal fluctuations in the low-Earth orbit (LEO) and spacecraft attitude maneuvers. Over the long exposures associated with x-ray observing, such fluctuations might impair HXI image quality unless a compensation technique is employed. To provide the required corrections, the Canadian contribution is a laser metrology system (the Canadian ASTRO-H Metrology System, CAMS) aiming at measuring displacements in the alignment of the HXT optical path. Two laser and detector modules (CAMS-LD-1 and CAMS-LD-2) are located on the top plate of the FOB, and two passive target modules (CAMS-T-1 and CAMS-T-2), each consisting of a retroreflector (corner cube mirror), are mounted on the EOB detector plate (HXI plate).¹³

Almost all of onboard subsystems, such as the command/data handling system, the attitude control system, and four types of x-ray/gamma-ray telescope instruments, are connected to the SpaceWire network using a highly redundant topology.¹⁴ The number of physical SpaceWire links among components exceeds 140 connecting ~ 40 separated components (i.e., separated boxes), and there are more links in intracomponent (intraboard) networks. Most of the electronics boxes of both the spacecraft bus and the scientific instruments are mounted on the side panels of the spacecraft. The electronics boxes for the HXI are mounted on the HXI plate and the side panels of the spacecraft. The spacecraft carried the GPS receiver, whose timing was synchronized among electronics under the SpaceWire network within the $35\text{-}\mu\text{s}$ accuracy.¹⁵ The overall timing performance has been verified in orbit at about $300\text{-}\mu\text{s}$ absolute accuracy by the simultaneous observation of a neutron-star pulsar with the Kashima NICT radio observatory.¹⁶

3 On-Orbit Operation

ASTRO-H was injected into an approximately circular orbit with an altitude of 575 km and an inclination of 31 deg (Table 2). The launch operation went smoothly, and the orbit was exactly as planned. ASTRO-H was named Hitomi, which means the pupil of the eye in Japanese, and it was hoped that the observatory will function as a powerful eye to look into the x-ray emitting processes operating in a wide range of objects. As mentioned before, the Hitomi satellite lost contact with the ground on March 26. The reports on the analysis of the cause of the anomalous events are given on the JAXA homepage.¹⁷

After initial operations of the spacecraft, including the tuning of the attitude control system and the start-up of the SXS coolers, we commenced operation of the EOB at the end of which the HXI plate was mounted. On February 27, we turned on the electronics of the EOB (EOB-E). On the same day, lasers of two CAMS-LD were turned on, in order to monitor the orientation of the EOB during its deployment. On the next day, we started deployment of the EOB. Since the HXI plate was quite massive, ~ 150 kg in total, a lateral shake developed by degrees as the EOB mast was being extended. This is because the mast is not stiff enough during deployment to sustain the massive

Table 1 Key parameters of the payload.

Parameter	HXI	SXS	SXI	SGD
Detector technology	Si/CdTe cross-strips	Microcalorimeter	X-ray CCD	Si/CdTe Compton Camera
Focal length	12 m	5.6 m	5.6 m	—
Effective area	300 cm ² at 30 keV	300 cm ² at 6 keV 250 cm ² at 1 keV	350 cm ² at 6 keV 370 cm ² at 1 keV	>20 cm ² at 100 keV Compton mode
Number of pixels	128 strips orthogonally	6 × 6	(640 × 640) × 4 chips	—
Energy range	5 to 80 keV	0.3 to 12 keV	0.4 to 12 keV	60 to 600 keV
Energy resolution (FWHM)	<2 keV (at 60 keV)	<7 eV (at 6 keV)	<200 eV (at 6 keV)	<4 keV (at 60 keV)
Angular resolution	1.7 arc min (at 30 keV)	~1.2 arc min	~1.3 arc min	—
Effective field of view	~9 × 9 arc min ²	~3 × 3 arc min ²	~38 × 38 arc min ²	<0.6 × 0.6 deg ² (<150 keV)
Time resolution	25.6 μs	5 μs	4/2/0.5/0.1 s	25.6 μs
Operating temperature	−25°C	50 mK	−120°C	−20°C

Table 2 Hitomi mission.

Launch site	Tanegashima Space Center, Japan
Launch vehicle	JAXA H-IIA rocket
Orbit altitude (apogee)	576.5 km
Orbit altitude (perigee)	574.4 km
Orbit type	Approximate circular orbit
Orbit inclination	31 deg
Total length	14 m
Mass	2.7 metric ton
Power	<3500 W

HXI plate since the mast is composed of multiple joints and hence has some mechanical looseness. Accordingly, lateral angular velocity sometimes approached a software limit, so we carried out the deployment intermittently. We achieved the final full extension configuration of the EOB using four orbits. All operations were performed when the satellite was in contact with the ground station in Japan.

In Fig. 3(a), we show the time history of the center position of the EOB (EOB-X and EOB-Y), its rotation around the spacecraft Z-axis from the nominal orientation, and an apparent unbiased distance (EOB-r12p) throughout Hitomi's life from the start of the EOB extension. EOB-r12p is a difference between measured and actual distance between two corner cubes. The times of satellite-attitude maneuvers are drawn with the vertical lines. The time of the EOB extension is clearly marked by a jump of the center positions of the HXI plate measured by CAMS. After that, however, the location of the HXI plate is mostly within 0.5 mm in peak-to-bottom (note that

10 arc sec at a distance of 12 m is 0.582 mm). Within a single observation (during time interval of two adjacent maneuvers), jitter of the HXI plate is as small as ~0.2 mm. This is comparable or smaller than the pixel size of the HXI (0.25 mm). The stability of the image at the focal plane was monitored with CAMS. As shown in Fig. 3(b), the movement of the focal plane image is <400 μm corresponding to about 7 arc sec. We conclude that we achieved a highly stable EOB.

The microcalorimeter array of SXS has a linear size of 5 mm and is located at the focal plane of the telescope SXT-S. This gives the angular size covered by SXS to be 3 arc min. For the HXT, with focal length 12 m, the effective area at 1 arc min offset from the optical axis is about 80% at 50 to 60 keV. Therefore, the vignetting at 1 arc min off-axis is about 20%. The mutual alignment to enable both SXS and HXI to observe an object right at the optical axes of the telescopes took a lot of effort. As a result, the pointing of an object at the center of the SXS instrument gave images right at the expected positions for the SXI, HXI1, and HXI2 instruments.

Since Hitomi was in an LEO, with the attitude pointed to a direction in the inertial frame, the satellite conditions change throughout one orbit. The temperature gradient changes depending on the day and night phases, and the albedo from the earth and also gravity gradient on the spacecraft change largely in the orbit. To fulfill the requirement of the pointing control accuracy of ~60 arc sec, the thermal design needs to be very precise.¹² The temperatures measured by Heater Control Electronics sensors at various spacecraft positions were all within the acceptable range. Also, temperature data after the start-up of mission instruments, after March 20, were mostly within 5°C of the predicted values.¹⁸ There are differences of 7°C in some instruments, but no data show deviations larger than 10°C.

Along with the parameter tuning operation for the satellite bus and the attitude system, we observed several x-ray sources. The main purpose of the observations was the calibration of x-ray instruments, but the sources also provided interesting scientific data. The observed sources are the Perseus cluster (February 25 to 27, March 4 to 8), N132D (March 8 to 11),

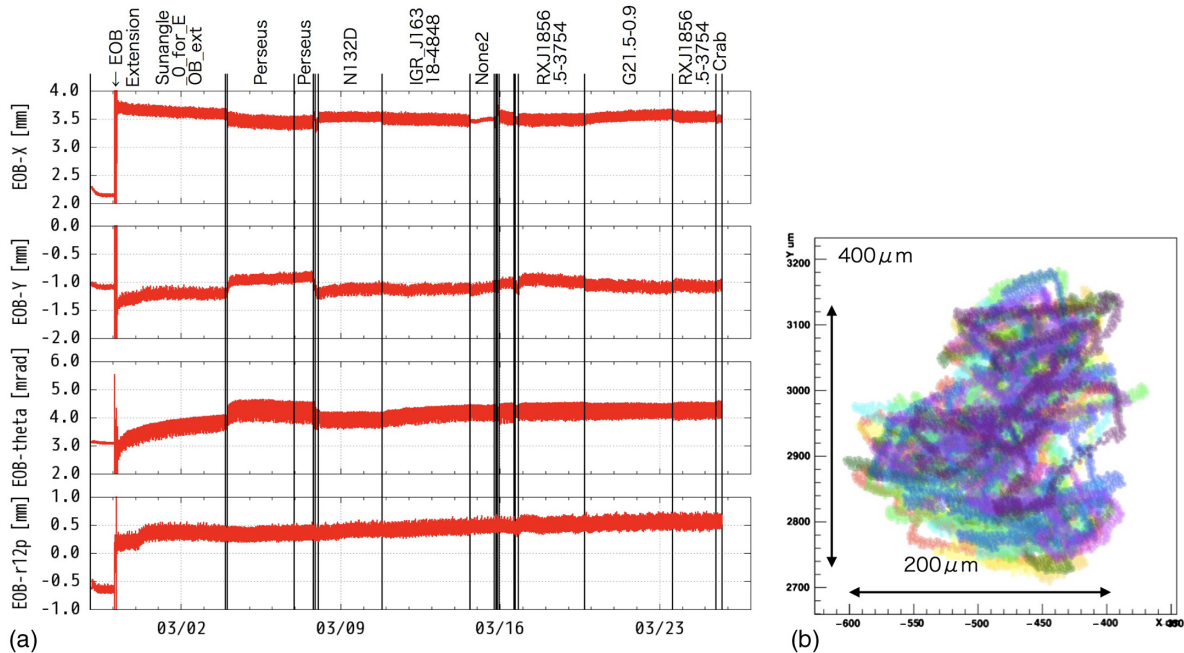


Fig. 3 (a) The time history of the center position of the EOB (EOB-X and EOB-Y), its rotation around the spacecraft Z-axis (the launch direction) from the nominal orientation, and changes of the distance between the two corner cubes. (b) Stability of the focal plane alignment measured in about a day with CAMS after the EOB extension.

IGR J16318-4848 (March 11 to 15), RX J1856-3754 (March 17 to 19, 23 to 25), G21.5-0.9 (March 19 to 23), and the Crab Nebula (March 25). The SXS was operational before the Perseus cluster observation, and SXI started observation during the pointing to Perseus. The HXI1 and HXI2 were started on March 8 to 15 and SGD on March 16 to 25. All the instruments finished their start-up operations on the day before the loss of contact. The Hitomi data will be archived in the public archive at the DARTS (JAXA/ISAS) and HEASARC (NASA/GSFC) after 1-year propriety period that starts when the final data processing is completed.¹⁹

The first light observation of the Perseus cluster unequivocally showed the superb spectroscopic performance of the SXS by revealing the narrow line complex of He-like ion of iron around 6.7 keV from the core of the Perseus cluster.²⁰

4 Science Instruments

Instruments onboard the Hitomi Satellite include a high-resolution, high-throughput spectrometer (SXS) sensitive over 0.3 to 12 keV with high spectral resolution of $\Delta E < 7$ eV (FWHM), enabled by a microcalorimeter array located in the focal plane of thin-foil x-ray optics; hard x-ray imaging spectrometers (HXI) covering 5 to 80 keV, located in the focal plane of multilayer-coated, focusing hard x-ray mirrors (HXT); a wide-field imaging spectrometer sensitive over 0.4 to 12 keV, with an x-ray CCD camera (SXI) in the focal plane of a SXT; and a nonfocusing Compton camera-type SGD, sensitive in the 60- to 600-keV band.

In the following sections, these instruments are briefly described. Detailed descriptions of the instruments and their current status are available in other papers.

4.1 Soft X-ray Telescopes

The SXT^{21–25} is very similar to the Suzaku X-ray Telescope²⁶ but with a longer focal length of 5.6 m and a larger outer diameter of 45 cm. The SXT consists of three parts: an x-ray mirror, a stray light baffle called the pre-collimator, and a thermal shield to keep the mirror temperature at around 20°C. The mirror is a conically approximated Wolter I grazing incidence optic with 203 nested shells. Each shell is segmented into four quadrants.

The flight SXT mirror assemblies [Fig. 4(a)], SXT-I for the SXI and SXT-S for the SXS, were fabricated at NASA/GSFC and delivered to JAXA. According to calibration at GSFC and ISAS, the angular resolution [half-power diameter (HPD)] is 1.3 and 1.2 arc min for the SXT-I and SXT-S, respectively. The result obtained with SXT-S exceeds the desired goal. Effective areas were measured to be ~ 590 cm² at 1 keV and ~ 430 cm² at 6 keV. The system net effective area at 1 and 6 keV is about 250 and 300 cm² for the SXS and 370 and 350 cm² for the SXI, respectively. However, since the SXS gate valve (GV) was closed during observations, the SXS effective area was reduced by the Be window transmission and the GV obscuration. The SXS net effective area with the GV closed was about 160 cm² at 6 keV with almost no area below 2 keV.

According to the in-flight data, the SXT-I and SXT-S were clearly focusing x-rays onto the corresponding detectors and they seemed to be working as expected. The overall effective area (flux) was examined using the Crab and the G21.5-0.9 data. Model fittings for both spectra produced a power-law photon index consistent with the previous measurements,^{27,28} which indicates that the effective area response was consistent with the ground calibration results.²⁹ The measured HPD was 1.3 and 1.2 arc min for SXT-I and SXT-S, respectively. Detailed in-flight performance of the SXT is presented in other publications.³⁰

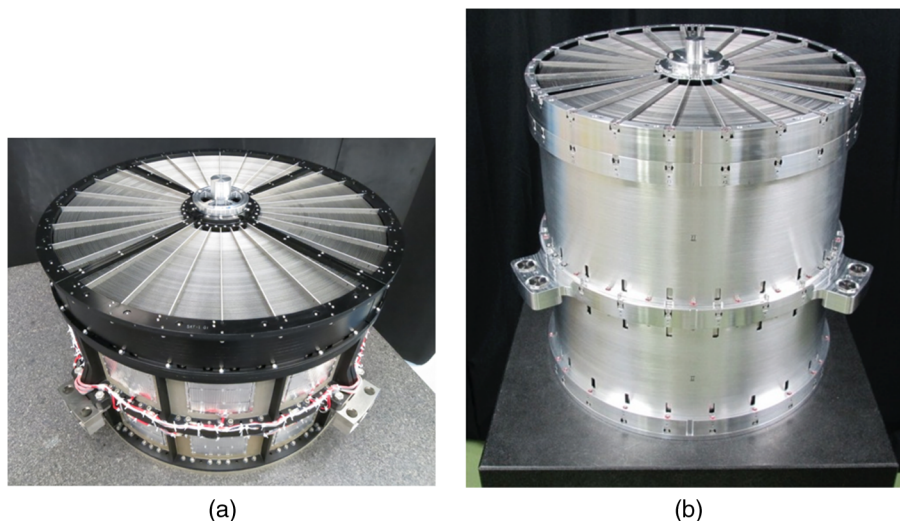


Fig. 4 Photographs of flight models of (a) Soft X-ray Telescope, SXT-S, and (b) Hard X-ray Telescope, HXT-1.

4.2 Hard X-ray Telescopes

A depth-graded multilayer mirror reflects x-rays not only by total external reflection but also by Bragg reflection. To obtain a high reflectivity up to 80 keV, the HXT consists of a stack of multilayers with different sets of periodic length and number of layer pairs with a platinum/carbon coating. The technology of a hard x-ray focusing mirror has already been proven by the balloon programs InFOC μ S (2001, 2004),^{31,32} HEFT (2004),³³ SUMIT (2006),³¹ and recently with the NuSTAR satellite.³⁴

The HXT^{35–40} consists of three parts: an x-ray mirror, a stray light baffle (pre-collimator), and a thermal shield [Fig. 4(b)]. The mirror is based on conically approximated Wolter I grazing incidence optics.^{37,38} The diameters of the innermost and the outermost reflectors are 120 and 450 mm, respectively. The total number of nested shells is 213. Since a telescope module is made up from three segments with an azimuthal opening angle of 120 deg each, it requires 1278 reflectors in total. Production of two flight-ready HXT mirror assemblies, HXT-1 and HXT-2, was completed in 2014. According to calibration performed using the beam line BL20B2 of the synchrotron radiation facility SPring-8, the characteristics of HXT-1 and HXT-2 are quite similar. Based on the ground calibration at the SPring-8, a collecting area of 174 cm² at 30 keV for one telescope has been achieved, resulting in a total effective area of 348 cm². The HPD of the HXTs is ~ 1.9 arc min at 30 keV.^{40,41} After the launch, the characteristics of HXTs were evaluated using observational data of the Crab Nebula. The HPDs of HXT-1 and HXT-2 in the 5- to 80-keV band were 1.59 and 1.65 arc min, respectively. Note, however, that the encircled energy function (EEF) was normalized at $r = 6$ arc min on the ground whereas, due to the limitation of the HXI field of view, the in-flight EEF was normalized at $r = 4$ arc min and the data in the area $r > 4$ arc min were subtracted as background. We, therefore, reprocessed the ground calibration data in the same way as the in-flight data. The reanalyzed HPDs at 30 keV were 1.77 and 1.84 arc min for HXT-1 and HXT-2, respectively. The in-flight HPDs seem to be slightly smaller than the ground ones. However, both the in-flight and ground HPDs can have an uncertainty of 0.1 arc min. Thus, they are consistent with each other within the uncertainty. The unabsorbed flux of the Crab

nebula in the 3- to 50-keV band was measured to be 3.59×10^{-8} erg s⁻¹ cm⁻² with HXT-1 and 3.55×10^{-8} erg s⁻¹ cm⁻² with HXT-2. These values are slightly ($\sim 5\%$) larger than that measured with NuSTAR. Detailed in-flight performance of the HXT is presented in other publications.⁴²

4.3 Soft X-ray Spectrometer System

The SXS system consists of the SXT, the filter wheel (FW) assembly,⁴³ and the SXS.^{44–47} The SXS is a 36-pixel system with an energy resolution of better than 7 eV between 0.3 and 12 keV. The array design for the SXS is basically the same as that for the Suzaku XRS⁴⁸ but has larger pixel pitch and absorber size. HgTe absorbers are attached to ion-implanted Si thermistors formed on suspended Si microbeams.^{49–51} The 6×6 array of silicon thermistors on an 832- μ m pitch was manufactured during the Suzaku/XRS program along with arrays with smaller pitch as an option for a larger field of view [Fig. 5(a)]. For SXS, improved heat sinking was added to the frame of the array, and HgTe absorbers with very low specific heat were attached to the pixels. The width of the individual absorbers was 819 μ m.⁵¹ A square-cm anticoincidence detector was installed behind the microcalorimeter array in the detector assembly. The detector assembly consisted of the detector enclosure and its mechanical, thermal, and electrical interfaces, including the first stage of amplification.

The SXS detector assembly and low-temperature coolers were installed in the dewar [Fig. 5(b)]. The cooling system was required to cool the array to 50 mK with sufficient duty cycle to fulfill the SXS scientific objectives. This restriction requires extremely low heat loads. To achieve the necessary gain stability and energy resolution, the cooling system must regulate the detector temperature, to within 2- μ K rms over intervals of about half an hour, for at least 24 h/cycle.⁵² From the detector stage to room temperature, the cooling chain is composed of a three-stage adiabatic demagnetization refrigerator (ADR),⁵³ superfluid liquid ⁴He (hereafter LHe), a ⁴He Joule-Thomson (JT) cryocooler, and two-stage Stirling cryocoolers.

To obtain a good performance for bright sources, an FW assembly, which includes a wheel with selectable filters and a set of modulated x-ray sources, were provided by SRON

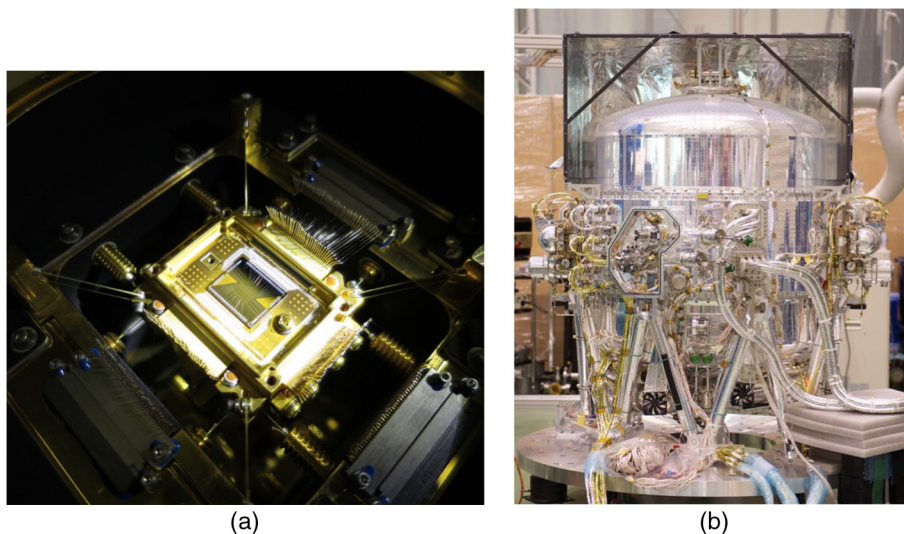


Fig. 5 Photographs of (a) SXS sensor and (b) SXS dewar. The sensor was suspended from the outer structure using Kevlar, and electrical connections to the housing were made using tensioned wires to reduce the sensitivity to microphonics. The outer shell of the dewar is 950 mm in diameter.

and the University of Geneva. This was placed at a distance of 90 cm from the detector. The FW is able to rotate a suitable filter into the beam to optimize the quality of the data, depending on the source characteristics.⁴³ In addition to the filters, a set of on-off-switchable x-ray calibration sources, using a light-sensitive photocathode, were available. With these calibration sources, the energy scale could be calibrated with a typical 1- to 2-eV accuracy, allowing proper gain and linearity calibration of the detector in-flight.

All SXS components except for the SXS power distributor (SXS-DIST) were powered off at launch (cold launch). The first critical operation was to re-establish the He plumbing in space.⁵⁴ Quickly after the fairing opened, the He vent valve was opened, which was confirmed by the telemetry during the first contact 50 min after the launch. We next focused on starting the cooling chain. On day 0, we started two shield coolers at the full wattage and two precoolers (PC) at a low wattage. On day 1, the PCs were also ramped up to the full wattage. By day 4, the JT cooler was also ramped up step by step. On day 5, the ADR cool down was started and the sensor was cooled to 50 mK. After that, the cooling chain worked without any problem until the end of the mission by repeating ADR cycles periodically and continuously operating the cryocoolers.

The signal chain was also started within the first week. On day 2, both the analog and digital signal processors were started (called XBOX and PSP, respectively). After the initial check and the parameter setting, the first noise measurement was performed on day 2 at a warm detector temperature and on day 5 at the 50-mK temperature.

The SXS was ready for observations by as early as day 6. On day 7, the spacecraft was pointed to the Perseus cluster, and we observed x-rays from an astronomical target for the first time. Although the pointing was offset from the cluster core by a few arc minutes, we obtained sufficient counts to make an offset correction based on our own count rate map within a few cycles. On day 8, an adjustment maneuver was made toward the core of the cluster for a longer exposure time. The detector NXB level measured during the Earth occultation was very low ($<1.0 \times 10^{-3}$ cts s^{-1} keV $^{-1}$).

After the EOB extension, we started commissioning the FW electronics, which was the last SXS subsystem to be powered. The FW was rotated on day 30 to provide x-ray illumination of the whole array by ^{55}Fe sources. The resulting calibration data set was used to refine the gain scales and measure the energy resolutions of the individual pixels. Figure 6(a) is a histogram of the distribution of resolutions measured across the array. The composite resolution of the whole array was 4.9 eV (FWHM) [Fig. 6(b)].^{51,55,56}

What remained to be done during the commissioning phase but was not completed were: (i) the start-up of the modulated x-ray source, (ii) opening of the GV and the start of the temperature control of the dewar main shell filter, and (iii) the final setting of the event threshold. The cryogen-free operation using the third stage ADR, which was planned in later phase of the mission,⁵⁷ was also not carried out.

4.4 Soft X-ray Imager

X-ray sensitive silicon CCDs are key detectors for x-ray astronomy. The low background and high-energy resolution combined with wide field of view achieved with the Suzaku XIS clearly shows that the x-ray CCD can also play a very important role in the mission. The soft x-ray imaging system consists of an x-ray mirror, the SXT-I, and a CCD camera, the SXI.^{58–63,64} Figure 7(a) shows a photograph of the SXI detector. The SXI camera contains a cold plate on which four CCDs are placed. The cold plate is connected to two identical single-stage Stirling coolers.

Start-up operation of SXI began from March 2, 2016. The CCD temperature reached the nominal value, -110°C , on March 7, and we started data acquisition in the event mode. One of the Stirling coolers was used to cool down the CCDs. Fine control of the temperature was performed with heaters attached to the cold plate, and we confirmed the same level of temperature stability as that during the ground tests. We employed a charge injection technique from the beginning of the operation to cope with the decrease of the charge transfer efficiency due to radiation damage. Artificial charge was injected from the top of columns of the CCDs at every 160 rows

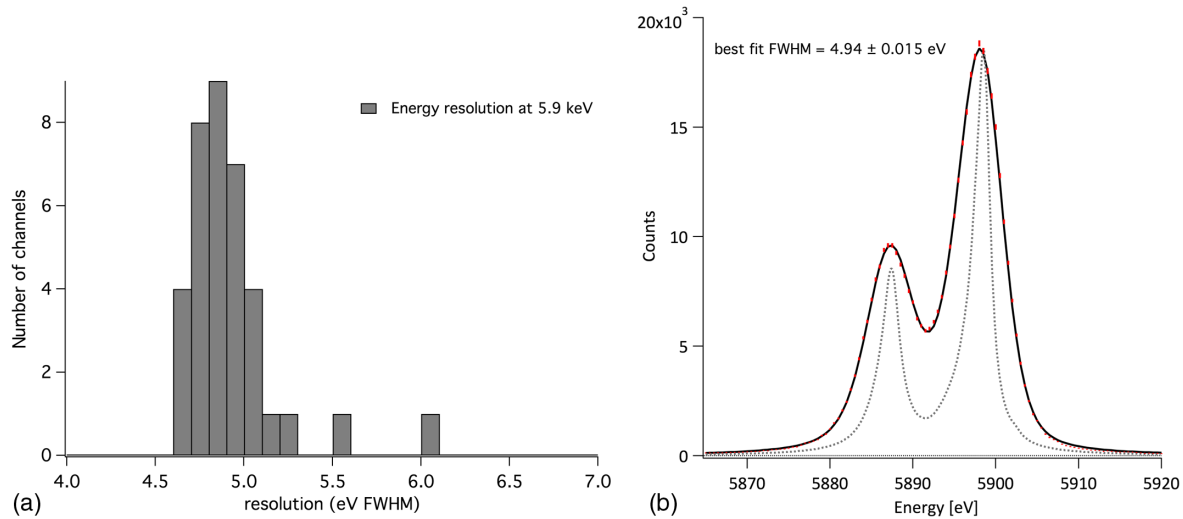


Fig. 6 (a) A histogram of the distribution of resolutions measured across the array. (b) The whole-array spectrum around 5.9 keV. The points are the data, with \sqrt{N} error bars on the counts barely visible. The dark line is the best fit to a model of the natural line shape convolved with Gaussian broadening, and the dashed grey line is the natural line shape.

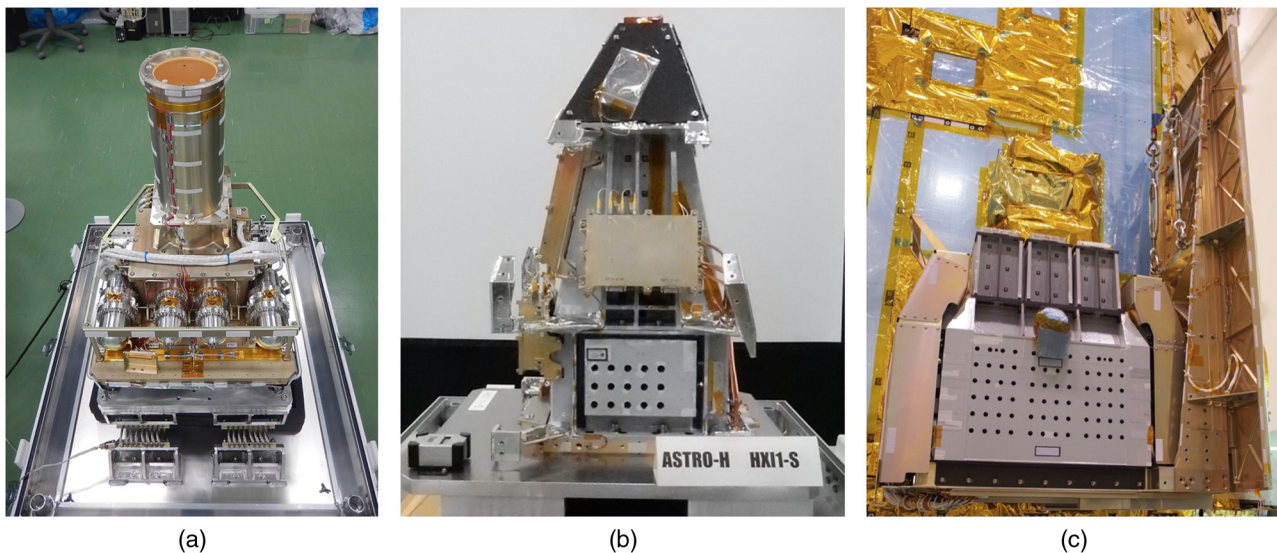


Fig. 7 Photographs of (a) SXI, (b) HXI, and (c) SGD.

(before the on-chip 2×2 binning). We confirmed that the noise level of CCDs was about 5 to 7 e^- rms, the same as that of the ground tests. We also confirmed that the amount of the injected charge was not changed from the ground test.

The first target was the Perseus cluster of galaxies. As shown in Fig. 8(a), the cluster image is offset from the SXI center, because the CCDs were placed to have an offset relative to the aim point of SXT-I by 5 arc min to avoid the CCD gaps. Two calibration sources of ^{55}Fe are also seen as semicircular shapes on top and bottom centers. Initial performance of the SXI was checked using these calibration source data and the Perseus data. The gain and the energy resolution of the CCDs were found to be roughly consistent with the ground data.⁶⁵ Thus, we confirmed that the SXI functioned properly on orbit. We accumulated background data from the source-free regions of the SXI field of view. In the case of Suzaku

XIS(BI),⁶⁶ non-x-ray background NXB increased rapidly above 6 keV. Such an increase of NXB almost disappeared for the SXI due to the thick depletion layer (200 μm) compared to that of the XIS(BI) ($\sim 42 \mu\text{m}$). Furthermore, the Ni K lines in the NXB spectrum became much weaker while the Au L lines became more prominent.

4.5 Hard X-ray Imager

There are two HXI sensor modules: HXI1-S and HXI2-S [Fig. 7(b)]. The imager part of the HXI⁶⁷⁻⁷⁴ consisted of four layers of 0.5-mm-thick double-sided silicon strip detectors (DSSD) and one layer of newly developed 0.75-mm-thick CdTe double-sided cross-strip detector (CdTe-DSD). In this configuration, soft x-ray photons below ~ 30 keV are absorbed in the Si part, and hard x-ray photons above ~ 30 keV go through the Si

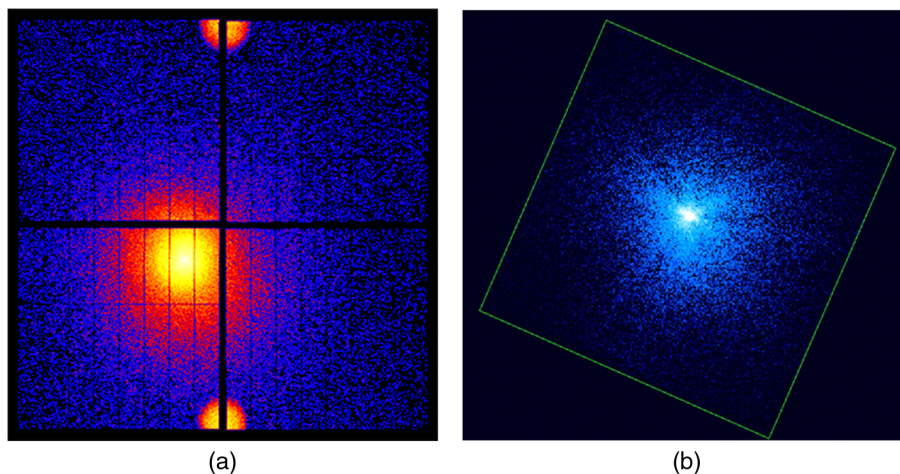


Fig. 8 (a) Logarithmically scaled image of the Perseus cluster. Its core is just on the aim point of the SXI. Two calibration areas are seen as bright regions on top and bottom center. The size of the image is 38×38 arc min².⁶³ (b) A logarithmically scaled image of the Crab Pulsar for 10- to 50-keV energy band, extracted from the HXI1 data of the Crab observation. The square in the image corresponds to the 9.1×9.1 arc min² FOV of the HXI. Note that the correction of the satellite attitude is preliminary and vignetting correction is not applied.⁶⁷

part and are detected by the CdTe part. To reduce the background, the sensor part is surrounded by a thick active shield and collimator made of bismuth germanate (BGO) scintillator coupled to avalanche photodiodes (APDs). In addition to the increase in efficiency, the stack configuration and individual readouts per each layer provide information on the interaction depth. This depth information is very useful for reducing the background in space applications, because we can expect that low-energy x-rays interact in the upper layers and, therefore, it is possible to reject the low-energy events, mainly due to the NXB, detected in lower layers. The $E < 30$ keV spectrum, obtained with the Si DSSD, has a much lower background due to the absence of activation in heavy material, such as Cd and Te. The DSSDs cover the energy below 30 keV while the CdTe strip detector covers the 30- to 80-keV band.

The electronics boxes of the HXIs (HXI-DE, DPU, and AE) were powered on February 28 to 29. Then, the HXI sensor (HXI-S) parts temperature was gradually decreased from 5°C to -25°C followed by the bias voltage operation of HXI1-S starting on March 8. The APD bias, Si DSSD bias, and CdTe DSD bias were raised to their operational voltage step by step, and the HXI1-S became operational on March 12. The HXI2-S followed on March 14. All 1280 readout channels for each of the HXI1-S and HXI2-S imager performed well, showing noise performance consistent with the prelaunch on-ground measurements. An image of the Crab Pulsar taken with HXI1 is shown in Fig. 8(b).^{67,75}

In addition to the thick BGO active shield and the concept of multilayer configuration of the imager, CXB baffling within the detector and inside the spacecraft worked well to reduce the background. The HXI achieved a low background level of $1 - 3 \times 10^{-4}$ cnt s⁻¹ cm⁻² throughout their energy band of 5 to 80 keV, except for at a few energy region of activation lines in CdTe (here, the flux is normalized by the geometrical size of the detector, 10 cm²), which is the lowest level ever achieved in orbit. Due to the optimum design of the HXT and the long focal length of 12 m, the effective area was also the largest among the hard x-ray imaging spectroscopy instruments, flown to date. The HXI showed the potential to

provide the highest sensitivity in this energy band, especially for diffuse sources.

4.6 Soft Gamma-Ray Detector

Figure 7(c) shows a photograph of the SGD detector module. The SGD⁷⁶⁻⁸¹ measures soft γ -rays via reconstruction of Compton scattering in the semiconductor Compton camera, covering an energy range of 60 to 600 keV with a sensitivity at 300 keV, being 10 times better than that of the Suzaku Hard X-ray Detector,^{82,83} by adopting a new concept of a narrow-FOV Compton telescope, combining Compton cameras and active well-type shields. There are two SGD sensor modules: SGD1 and SGD2. The Compton camera is made of 32 layers of 0.625-mm-thick Si pad detectors and 8 layers of 0.75-mm-thick CdTe pad detectors. The side of Si detectors is also surrounded by two layers of CdTe detectors. In the Si/CdTe Compton camera, events involving the incident γ -ray being scattered in the Si detectors and fully absorbed in the CdTe detectors are used for Compton imaging. The direction of the γ -ray is calculated by solving the Compton kinematics with information concerning deposit energies and interaction positions recorded in the detectors. In principle, each layer could act not only as a scattering part but also as an absorber part. A very compact, high-angular resolution (finesse of image) camera is realized by fabricating semiconductor imaging elements made of Si and CdTe, which have excellent performance in position resolution, high-energy resolution, and high-temporal resolution.

The camera was then mounted inside the bottom of a well-type active shield, made of BGO scintillators. The major advantage of employing a narrow FOV is that the direction of incident γ -rays is constrained to be inside the FOV. If the Compton cone, which corresponds to the direction of incident gamma rays, does not intercept the FOV, we can reject the event as background. Most of the background can be rejected by requiring this condition. The opening angle provided by the BGO shield is ~ 10 deg at 500 keV. An additional PCuSn collimator restricts the field of view of the telescope to 33' for photons below

100 keV, to minimize the flux due to the cosmic x-ray background in the FOV.

The power-on operation of SGD-DE, SGD-DPU, and SGD-AE was performed on March 1, 2016.^{81,84} After this operation, SGD HK telemetries, including temperature monitors of SGD-S, were generated. Then, the SGD-S was gradually cooled down to -25°C from March 3 to 13 by changing the SGD heater settings. Start-up operation of SGD-S began on March 15, 2016. First, Compton cameras, APD CSAs for BGO readout, and HV modules for Compton cameras and APDs were powered on, and then we applied the high-voltage step by step and set up detectors into the nominal observation mode. From March 21, SGD1-S had been operated in the nominal observation mode, and SGD2-S was shifted into the nominal observation on March 24, 2016. Basic performance of the SGD was confirmed in the Crab observation, albeit with very short exposure.

5 Summary

Carrying onboard the two types of x-ray optics and the four types of detectors, Hitomi (ASTRO-H) was designed to provide exciting wideband and high-energy-resolution data on various high-energy astrophysical objects. Its one month of operation in orbit demonstrated that many of the technologies introduced to the Hitomi mission worked well. In fact, all instruments produced data with satisfactory quality, though for a short period, until the loss of spacecraft capability. In particular, the acquired data clearly verified the key properties of the SXS, i.e., the high spectral resolution (4.9-eV FWHM) for both point and diffuse sources over a broad 0.3- to 12-keV bandpass, with the low non-x-ray background ($<1.0 \times 10^{-3}$ cts s^{-1} keV $^{-1}$). Although the GV was not opened, the effective area was consistent with the designed value, indicating that an effective area of 250 cm^2 at 1 keV and 300 cm^2 at 6 keV would be achieved if the GV was open. Hitomi has, thus, opened the door to a generation of x-ray astronomy; forthcoming scientific papers based on the limited amount of data will clearly show the power of this challenging mission.

Acknowledgments

We thank the support from the JSPS Core-to-Core Program. We acknowledge all the JAXA members who have contributed to the ASTRO-H (Hitomi) project. All U.S. members gratefully acknowledge support through the NASA Science Mission Directorate. Stanford and SLAC members acknowledge support via DoE contract to SLAC National Accelerator Laboratory No. DE-AC3-76SF00515. Part of this work was performed under the auspices of the U.S. DoE by LLNL under Contract No. DE-AC52-07NA27344. Support from the European Space Agency is gratefully acknowledged. French members acknowledge support from the Centre National d'Études Spatiales. SRON is supported by NWO, the Netherlands Organization for Scientific Research. Swiss team acknowledges support of the Swiss Secretariat for Education, Research and Innovation. The Canadian Space Agency is acknowledged for the support of Canadian members. We acknowledge support from JSPS/MEXT KAKENHI Grant Nos. JP15H00773, JP15H00785, JP15H02070, JP15H02090, JP15H03639, JP15H03641, JP15H03642, JP15H05438, JP15H06896, JP15J02737, JP15K05107, JP15K17610, JP15K17657, JP16H00949, JP16H03983, JP16H06342, JP16J00548, JP16J02333, JP16K05295, JP16K05296, JP16K05300, JP16K05309, JP16K13787, JP16K17667, JP16K17672, JP16K17673,

JP17H02864, JP17K05393, JP21659292, JP23340055, JP23340071, JP23540280, JP24105007, JP24244014, JP24540232, JP25105516, JP25109004, JP25247028, JP25287042, JP25400236, JP25800119, JP26109506, JP26220703, JP26400228, JP26610047, and JP26800102. The following NASA Grants are acknowledged: NNX15AC76G, NNX15AE16G, NNX15AK71G, NNX15AU54G, NNX15AW94G, and NNG15PP48P to Eureka Scientific. This work was partly supported by Leading Initiative for Excellent Young Researchers, MEXT, Japan, and also by the Research Fellowship of JSPS for Young Scientists. H. Akamatsu acknowledges support of NWO via Veni grant. C. Done acknowledges STFC funding under Grant No. ST/L00075X/1. A. Fabian and C. Pinto acknowledge ERC Advanced Grant No. 340442. P. Gandhi acknowledges JAXA International Top Young Fellowship and UK Science and Technology Funding Council Grant No. ST/J003697/2. Y. Ichinohe, K. Nobukawa, and H. Seta are supported by the Research Fellow of JSPS for Young Scientists. N. Kawai is supported by the Grant-in-Aid for Scientific Research on Innovative Areas "New Developments in Astrophysics Through Multimessenger Observations of Gravitational Wave Sources." S. Kitamoto is partially supported by the MEXT Supported Program for the Strategic Research Foundation at Private Universities, 2014 to 2018. B. McNamara and S. Safi-Harb acknowledge support from NSERC. T. Dotani, T. Takahashi, T. Tamagawa, M. Tsujimoto, and Y. Uchiyama acknowledge support from the Grant-in-Aid for Scientific Research on Innovative Areas "Nuclear Matter in Neutron Stars Investigated by Experiments and Astronomical Observations." N. Werner is supported by the Lendület LP2016-11 Grant from the Hungarian Academy of Sciences. D. Wilkins is supported by NASA through Einstein Fellowship Grant No. PF6-170160, awarded by the Chandra X-ray Center, operated by the Smithsonian Astrophysical Observatory for NASA under Contract No NAS8-03060. We thank contributions by many companies, including in particular, NEC, Mitsubishi Heavy Industries, Sumitomo Heavy Industries, and Japan Aviation Electronics Industry. We acknowledge contribution and support by late Henri Aarts and Koujun Yamashita. It is our honor that we could have worked together with them for long years. Contributions by Takashi Kubota and Atushi Harayama are gratefully acknowledged. We note that this mission is supported by dedicated works of many graduate and undergraduate students from universities and research institutes participated in this project. Finally, we thank the following engineers ADNET Systems: Michael Witthoef, Kristin Rutkowski, Robert S. Hill, and Joseph Eggen; Wyle Information Systems: Andrew Sargent and Michael Dutka; SRON: Martin Frericks, Philippe Laubert, and Paul Lowes.

References

1. "NeXT Satellite Proposal," The NeXT Working Group, ISAS/JAXA, submitted (2003).
2. "NeXT Satellite Proposal," The NeXT Working Group, ISAS/JAXA, submitted (2005).
3. H. Kunieda, "Hard X-ray telescope mission (NeXT)," *Proc. SPIE* **5488**, 187 (2004).
4. T. Takahashi, K. Mitsuda, and H. Kunieda, "The NeXT mission," *Proc. SPIE* **6266**, 62660D (2006).
5. T. Takahashi et al., "The NeXT mission," *Proc. SPIE* **7011**, 701100 (2008).
6. T. Takahashi et al., "The ASTRO-H mission," *Proc. SPIE* **7732**, 77320Z (2010).

7. T. Takahashi et al., “The ASTRO-H observatory,” *Proc. SPIE* **8443**, 84431Z (2012).
8. T. Takahashi et al., “The ASTRO-H x-ray astronomy satellite,” *Proc. SPIE* **9144**, 914425 (2014).
9. SXS Proposal, “High resolution X-ray spectroscopy for the JAXA new exploration X-ray telescope,” NASA/GSFC, submitted to NASA (2007).
10. K. Ishimura et al. “Novel technique for spacecraft’s thermal deformation test based on transient phenomena,” *Trans. Jpn. Soc. Aeronaut. Space Sci. Aerosp. Technol. Jpn.* **12**(29), Pc_29–34 (2014).
11. T. Shimada et al., “Development status of electrical power subsystem for X-ray astronomy satellite ASTRO-H,” Tech. Rep. SANE2012-58, Vol. **112**, No. 229, pp. 17–22, IEICE Technical Committee, Minatoku, Tokyo (2012).
12. N. Iwata et al., “Thermal control system of x-ray astronomy satellite ASTRO-H: current development status and prospects,” in *44th Int. Conf. on Environmental Systems* (2014).
13. L. Gallo et al., “The Canadian ASTRO-H metrology system,” *Proc. SPIE* **9144**, 914456 (2014).
14. T. Yuasa et al., “A deterministic spacewire network onboard the ASTRO-H space X-ray observatory,” in *Proc. of Int. SpaceWire Conf.*, 8–10 November, Texas (2011).
15. Y. Terada et al. “The time assignment system and its performance aboard the Hitomi satellite,” *J. Astron. Telesc. Instrum. Syst.* **4**(2), 011206 (2017).
16. S. Koyama et al., “In-orbit timing calibration of Hitomi satellite with simultaneous observation of Crab,” *Publ. Astron. Soc. Jpn.*, submitted (2017).
17. http://global.jaxa.jp/projects/sat/astro_h/topics.html.
18. N. Iwata et al., “Evaluation of in-orbit thermal performance of X-ray astronomy satellite Hitomi,” *AIAA J. Spacecraft Rockets* **55**, 77–84 (2018).
19. L. Angelini et al., “ASTRO-H data analysis, processing and archive,” *Proc. SPIE* **9905**, 990514 (2016).
20. Hitomi Collaboration, “The quiet intracluster medium in the core of the Perseus cluster,” *Nature* **535**, 117–121 (2016).
21. T. Okajima et al., “Soft x-ray mirrors onboard the NeXT satellite,” *Proc. SPIE* **7011**, 70112X (2008).
22. P. Serlemitsos et al., “Foil x-ray mirrors for astronomical observations: still an evolving technology,” *Proc. SPIE* **7732**, 77320A (2010).
23. T. Okajima et al. “The first measurement of the ASTRO-H soft x-ray telescope performance,” *Proc. SPIE* **8443**, 844320 (2012).
24. Y. Soong et al. “ASTRO-H soft X-ray telescope (SXT),” *Proc. SPIE* **9144**, 914428 (2014).
25. T. Okajima et al. “First peak of ASTRO-H soft X-ray telescope (SXT) in-orbit performance,” *Proc. SPIE* **9905**, 99050Z (2016).
26. P. J. Serlemitsos et al., “The X-ray telescope onboard Suzaku,” *Publ. Astron. Soc. Jpn.* **59**, S9 (2007).
27. M. Kirsch et al., “Crab: the standard x-ray candle with all (modern) x-ray satellites,” *Proc. SPIE* **5898**, 589803 (2005).
28. M. Tsujimoto et al., “Cross-calibration of the X-ray instruments onboard the Chandra, INTEGRAL, RXTE, Suzaku, Swift, and XMM-Newton observatories using G21.5-0.9,” *Astron. Astrophys.* **525**, A25 (2011).
29. R. Iizuka et al., “Ground-based X-ray calibration of the Astro-H/Hitomi soft X-ray telescopes,” *J. Astron. Telesc. Instrum. Syst.* **4**(2), 011213 (2018).
30. P. J. Serlemitsos et al., “Design and fabrication of ASTRO-H (Hitomi) soft X-ray telescope—aluminum foil X-ray mirror,” in preparation (2017).
31. H. Kunieda et al., “Balloon-borne hard X-ray imaging observation of non-thermal phenomena,” *Proc. SPIE* **6266**, 62660B (2006).
32. Y. Ogasaka et al., “Thin-foil multilayer-supermirror hard x-ray telescopes for InFOCUS/SUMIT balloon experiments and NeXT satellite program,” *Proc. SPIE* **6688**, 668803 (2007).
33. F. Harrison et al., “Development of the high-energy focusing telescope (HEFT) balloon experiment,” *Proc. SPIE* **4012**, 693–699 (2000).
34. F. A. Harrison et al., “The nuclear spectroscopic telescope array (NuSTAR),” *Astrophys. J.* **770**, 103 (2013).
35. Y. Ogasaka et al., “The NeXT x-ray telescope system: status update,” *Proc. SPIE* **7011**, 70110P (2008).
36. H. Kunieda et al., “Hard X-ray telescope to be onboard ASTRO-H,” *Proc. SPIE* **7732**, 773214 (2010).
37. H. Awaki et al., “Current status of ASTRO-H hard x-ray telescopes (HXTs),” *Proc. SPIE* **8443**, 844324 (2012).
38. H. Awaki et al., “ASTRO-H hard X-ray telescope (HXT),” *Proc. SPIE* **9144**, 914426 (2014).
39. H. Awaki et al., “The hard X-ray telescope to be onboard ASTRO-H,” *Appl. Opt.* **53**, 7664–7676 (2014).
40. H. Awaki et al., “Performance of ASTRO-H hard X-ray telescope (HXT),” *Proc. SPIE* **9905**, 990535 (2016).
41. H. Mori et al., “On-ground calibration of the Hitomi Hard X-ray Telescopes,” *J. Astron. Telesc. Instrum. Syst.* **4**(2), 011210 (2018).
42. H. Matsumoto et al., “In-orbit performance of the Hard X-ray Telescope (HXT) on board Hitomi,” *J. Astron. Telesc. Instrum. Syst.* **4**(2), 011212 (2018).
43. C. P. de Vries et al., “Calibration sources for the soft x-ray spectrometer instrument on ASTRO-H,” *Proc. SPIE* **8443**, 844353 (2012).
44. K. Mitsuda et al. “The X-ray microcalorimeter on the NeXT mission,” *Proc. SPIE* **7011**, 701102K (2008).
45. K. Mitsuda et al. “The high-resolution x-ray microcalorimeter spectrometer system for the SXS on ASTRO-H,” *Proc. SPIE* **7732**, 773211 (2010).
46. K. Mitsuda et al. “Soft x-ray spectrometer (SXS): the high-resolution cryogenic spectrometer onboard ASTRO-H,” *Proc. SPIE* **9144**, 91442A (2014).
47. R. L. Kelley et al., “The ASTRO-H high-resolution soft x-ray spectrometer,” *J. Astron. Telesc. Instrum. Syst.*, in press (2018).
48. R. L. Kelley et al., “The Suzaku high resolution X-ray spectrometer,” *Publ. Astron. Soc. Jpn.* **59**, S77–S112 (2007).
49. R. L. Kelley et al., “Ion-implanted silicon X-ray calorimeters: present and future,” *J. Low Tem Phys.* **151**(1–2), 375–380 (2008).
50. F. S. Porter et al., “The detector subsystem for the SXS instrument on the ASTRO-H Observatory,” *Proc. SPIE* **7732**, 77323J (2010).
51. C. Kilbourne et al., “The design, implementation, and performance of the Astro-H SXS calorimeter array and anti-coincidence detector,” *J. Astron. Telesc. Instrum. Syst.* **4**(2), 011214 (2018).
52. R. Fujimoto et al., “Performance of the helium dewar and cryocoolers of ASTRO-H SXS,” *J. Astron. Telesc. Instrum. Syst.* **4**(2), 011208 (2018).
53. P. J. Shirron et al. “Design and on-orbit operation of the adiabatic demagnetization refrigerator on the ASTRO-H soft x-ray spectrometer instrument,” *J. Astron. Telesc. Instrum. Syst.*, in press (2018).
54. M. Tsujimoto et al., “In-orbit operation of the ASTRO-H SXS,” *J. Astron. Telesc. Instrum. Syst.* **4**(2), 011205 (2017).
55. Y. Takei et al., “Vibration isolation system for cryocoolers of Soft X-ray Spectrometer (SXS) onboard ASTRO-H (Hitomi),” *J. Astron. Telesc. Instrum. Syst.* **4**(2), 011216 (2018).
56. F. S. Porter et al., “In-flight performance of the soft x-ray spectrometer detector system on ASTRO-H,” *J. Astron. Telesc. Instrum. Syst.* **4**(2), 011218 (2018).
57. G. Sneiderman et al., “Cryogen-free operation of the Soft X-ray Spectrometer instrument,” *J. Astron. Telesc. Instrum. Syst.*, in press (2018).
58. T. G. Tsuru et al., “Soft X-ray Imager (SXI) onboard the NeXT satellite,” *Proc. SPIE* **6266**, 62662I (2006).
59. H. Tsunemi et al., “The SXI: CCD camera onboard the NeXT mission,” *Proc. SPIE* **7011**, 70110Q (2008).
60. H. Tsunemi et al., “The SXI: CCD camera onboard ASTRO-H,” *Proc. SPIE* **7732**, 773210 (2010).
61. K. Hayashida et al., “Soft x-ray imager (SXI) onboard ASTRO-H,” *Proc. SPIE* **8443**, 844323 (2012).
62. K. Hayashida et al., “Soft x-ray imager (SXI) onboard ASTRO-H,” *Proc. SPIE* **9144**, 914429 (2014).
63. H. Tsunemi et al., “Soft x-ray imager (SXI) on-board ASTRO-H,” *Proc. SPIE* **9905**, 990535 (2016).
64. T. Tanaka et al., “The soft X-ray imager (SXI) aboard the Hitomi satellite,” *J. Astron. Telesc. Instrum. Syst.* **4**(2), 011211 (2018).
65. H. Nakajima et al., “In-orbit performance of the soft X-ray imaging system aboard Hitomi,” *Publ. Astron. Soc. Jpn.* **70**(2), in press (2017).
66. K. Koyama et al., “X-Ray Imaging Spectrometer (XIS) on board Suzaku,” *Publ. Astron. Soc. Jpn.* **59**, S23–S33 (2007).
67. K. Nakazawa et al., “The hard x-ray imager (HXI) onboard ASTRO-H,” *J. Astron. Telesc. Instrum. Syst.*, in press (2018).
68. T. Takahashi et al., “Wide band X-ray imager (WXI) and soft gamma-ray detector (SGD) for the NeXT mission,” *Proc. SPIE* **5488**, 549–560 (2004).

69. K. Nakazawa et al., “Hard x-ray imager for the NeXT mission,” *Proc. SPIE* **6266**, 62662H (2006).
70. M. Kokubun et al., “Hard x-ray imager (HXI) for the NeXT mission,” *Proc. SPIE* **7011**, 70110R (2008).
71. M. Kokubun et al., “Hard x-ray imager for the ASTRO-H mission,” *Proc. SPIE* **7732**, 773215 (2010).
72. M. Kokubun et al., “Hard x-ray imager (HXI) for the ASTRO-H mission,” *Proc. SPIE* **8443**, 844325 (2012).
73. G. Sato et al., “The hard x-ray imager (HXI) for the ASTRO-H mission,” *Proc. SPIE* **9144**, 914427 (2014).
74. G. Sato et al., “The Si/CdTe semiconductor camera of the ASTRO-H Hard X-ray Imager (HXI),” *Nucl. Instrum. Methods*, **831**, 235–241 (2016).
75. K. Hagino et al., “In-orbit performance and calibration of the hard X-ray imager (HXI) onboard Hitomi,” *J. Astron. Telesc. Instrum. Syst.*, in press (2018).
76. T. Takahashi et al., “Hard X-ray and gamma-ray detectors for the NeXT mission,” *New Astron. Rev.* **48**, 309–313 (2004).
77. H. Tajima et al., “Soft gamma-ray detector for the ASTRO-H mission,” *Proc. SPIE* **7732**, 773216 (2010).
78. S. Watanabe et al., “Soft gamma-ray detector for the ASTRO-H mission,” *Proc. SPIE* **8443**, 844326 (2012).
79. Y. Fukazawa et al., “Soft gamma-ray detector for the ASTRO-H mission,” *Proc. SPIE* **9144**, 91442C (2014).
80. S. Watanabe et al., “The Si/CdTe semiconductor Compton camera of the ASTRO-H soft gamma-ray detector (SGD),” *Nucl. Instrum. Methods* **765**, 192–201 (2013).
81. S. Watanabe et al., “The soft gamma-ray detector (SGD) onboard ASTRO-H,” *Proc. SPIE* **9905**, 990536 (2016).
82. T. Takahashi et al., “Hard X-ray detector (HXD) on board Suzaku,” *Publ. Astron. Soc. Jpn.* **59**, S35–S51 (2007).
83. M. Kokubun et al., “In-orbit performance of the hard X-ray detector on board Suzaku,” *Publ. Astron. Soc. Jpn.* **59**, S53 (2007).
84. H. Tajima et al., “Design and performance of soft gamma-ray detector onboard the Hitomi (ASTRO-H) satellite,” *J. Astron. Telesc. Instrum. Syst.*, in press (2018).

Biographies for the authors are not available.